parameters is found for other types of NPs (Ag, $ZrO_2$, $TiO_2$, and $In_2O_3$) (fig. S6). These results show that to first approximation, and in agreement with MD simulations (*15*), the microscopic details of the NP surface only weakly influence the solvent restructuring. However, it is possible that the spread of data points in Fig. 2B, which increases for increasing alkyl chain length, indicates an additional role for particle shape, surface restructuring, or differences in capping agent. Our model of restructuring for ethanol at the surface of a ZnO NP decorated with citrate and hydroxyl groups of capping ligands is illustrated in Fig. 3. The surface coverage of NPs with organic ligand molecules is sufficient to prevent agglomeration but in fact is unexpectedly small according to neutron PDF data (*19*) and nuclear magnetic resonance (NMR) studies (*20*). MD simulations (*15*, *21*, *22*), in agreement with experimental evidence from NMR (*20*), suggest that the vast majority of ZnO surface sites are terminated by hydroxyl groups. These could form a hydrogen-bonded network with adjacent solvent molecules.

Because of the shift in the oscillation with the solvent size, we conclude that the alcohol molecules tend to align perpendicular to the NP surface. Their hydroxyl groups form hydrogen bonds with the ligand molecules and hydroxyl groups. The alkyl chains of the solvent point away from the NP surface. The next- and second-next–neighboring molecules align so that hydrogen bonds can be formed within the solvent, which results in alternating layers of methyl groups and hydroxyl groups, building layers of decreased and enhanced electron density, as depicted in Fig. 3. Adjacent molecules within such a layer would orient in parallel, as observed for liquid films (*23*). The extent of restructuring depends on the solvent size and packing ability. Here, the packing ability is comparable for our alcohols because the hydroxyl group is always in a terminal position and the alkane chain is not branched. A second-harmonic generation (SHG) study on the interaction of organic solvent and solute molecules with hydroxylated silica surfaces supports our hydrogen bonding model (*24*). This study also showed that nonpolar solvents rearrange at hydroxylated surfaces, which supports our observation that the nonpolar n-hexane restructures at the NP surfaces. However, SHG is only sensitive to broken symmetry at interfaces, whereas it cannot provide information on the decay of the restructuring into the bulk liquid, as evidenced by our dd-PDFs.

## REFERENCES AND NOTES


1. W. H. Zachariasen, *J. Chem. Phys.* **3**, 158–161 (1935).
2. D. L. Wertz, R. K. Kruh, *J. Chem. Phys.* **47**, 388–390 (1967).
3. C. J. Benmore, Y. L. Loh, *J. Chem. Phys.* **112**, 5877–5883 (2000).
4. A. Vrhovšek, O. Gereben, A. Jamnik, L. Pusztai, *J. Phys. Chem. B* **115**, 13473–13488 (2011).
5. G. W. Longman, G. D. Wignall, R. P. Sheldon, *Polymer (Guildf.)* **20**, 1063–1069 (1979).
6. B. Götzelmann, A. Haase, S. Dietrich, *Phys. Rev. E Stat. Phys. Plasmas Fluids Relat. Interdiscip. Topics* **53**, 3456–3467 (1996).
7. J. Israelachvili, *Acc. Chem. Res.* **20**, 415–421 (1987).
8. I. K. Snook, W. van Megen, *J. Chem. Phys.* **72**, 2907 (1980).
9. O. M. Magnussen *et al.*, *Phys. Rev. Lett.* **74**, 4444–4447 (1995).
10. A. Doerr, M. Tolan, T. Seydel, W. Press, *Physica B* **248**, 263–268 (1998).
11. M. Mezger *et al.*, *Science* **322**, 424–428 (2008).
12. H. Reichert, P. J. Eng, H. Dosch, I. K. Robinson, *Phys. Rev. Lett.* **74**, 2006–2009 (1995).
13. D. T. Bowron, S. Díaz-Moreno, *J. Phys. Chem. B* **113**, 11858–11864 (2009).
14. R. Mancinelli, A. Botti, F. Bruni, M. A. Ricci, A. K. Soper, *Phys. Chem. Chem. Phys.* **9**, 2959–2967 (2007).
15. D. Spagnoli, J. P. Allen, S. C. Parker, *Langmuir* **27**, 1821–1829 (2011).
16. B. H. G. Hertz, I. An, *Angew. Chem. Int. Ed. Engl.* **9**, 124–138 (1970).
17. R. S. Cataliotti, F. Aliotta, R. Ponterio, *Phys. Chem. Chem. Phys.* **11**, 11258–11263 (2009).
18. Materials and methods are available as supplementary materials on *Science* Online.
19. K. Page, T. C. Hood, T. Proffen, R. B. Neder, *J. Appl. Cryst.* **44**, 327–336 (2011).
20. C. N. Valdez, A. M. Schimpf, D. R. Gamelin, J. M. Mayer, *ACS Nano* **8**, 9463–9470 (2014).
21. A. Kawska, P. Duchstein, O. Hochrein, D. Zahn, *Nano Lett.* **8**, 2336–2340 (2008).
22. D. Raymand, A. C. T. Duin, W. A. Goddard III, K. Hermansson, D. Spångberg, *J. Phys. Chem. C* **115**, 8573–8579 (2011).
23. H. K. Christenson, D. W. R. Gruen, R. G. Horn, J. N. Israelachvili, *J. Chem. Phys.* **87**, 1834 (1987).
24. X. Zhang, M. M. Cunningham, R. A. Walker, *J. Phys. Chem. B* **107**, 3183–3195 (2003).



## ACKNOWLEDGMENTS

We acknowledge the Bundesministerium für Bildung, Wissenschaft, Forschung und Technologie under grant 05K10WEB and a scholarship of the Friedrich-Alexander-University Erlangen-Nürnberg for financial support. Beam time at the European Synchrotron Radiation Facility and Argonne National Laboratory is gratefully acknowledged. We thank J. Hudspeth from beamline ID-15-B, European Synchrotron Radiation Facility, as well as K. Chapman and K. Beyer from beamline 11-ID-B, and Advanced Proton Source for support during our beamtime. We acknowledge A. Magerl and H. Reichert for discussions. All experimental raw data are stored at the European Synchrotron Radiation Facility. For access, please contact S.A.J.K. (kimber@esrf.fr).


## SUPPLEMENTARY MATERIALS

www.sciencemag.org/content/347/6219/292/suppl/DC1
Materials and Methods
Supplementary Text
Figs. S1 to S11
Table S1
References (*25*–*33*)


18 September 2014; accepted 26 November 2014
10.1126/science.1261412


PHYSICS

# Observation of Fermi arc surface states in a topological metal


**Su-Yang Xu,[1,2]* Chang Liu,[1]* Satya K. Kushwaha,[3] Raman Sankar,[4] Jason W. Krizan,[3] Ilya Belopolski,[1] Madhab Neupane,[1] Guang Bian,[1] Nasser Alidoust,[1] Tay-Rong Chang,[5] Horng-Tay Jeng,[5,6] Cheng-Yi Huang,[7] Wei-Feng Tsai,[7] Hsin Lin,[8] Pavel P. Shibayev,[1] Fang-Cheng Chou,[4,9] Robert J. Cava,[3] M. Zahid Hasan[1,2]†**



**The topology of the electronic structure of a crystal is manifested in its surface states. Recently, a distinct topological state has been proposed in metals or semimetals whose spin-orbit band structure features three-dimensional Dirac quasiparticles. We used angle-resolved photoemission spectroscopy to experimentally observe a pair of spin-polarized Fermi arc surface states on the surface of the Dirac semimetal $Na_3Bi$ at its native chemical potential. Our systematic results collectively identify a topological phase in a gapless material. The observed Fermi arc surface states open research frontiers in fundamental physics and possibly in spintronics.**


The realization of topological states of matter beyond topological insulators has become an important goal in condensed-matter and materials physics (*1*–*15*). In the topological insulators $Bi_{1-x}Sb_x$ and $Bi_2Se_3$ or topological crystalline insulators such as $Pb_{1-x}Sn_xTe(Se)$, the bulk has a full insulating energy gap, whereas the surface possesses an odd or even number of spin-polarized surface or edge states (*3*, *14*–*18*). These are symmetry-protected topological states (*19*). Very recently, the possibility of realizing new topological states in materials beyond insulators, such as metals or semimetals, has attracted much attention (*1*–*13*). Semimetals are materials whose bulk conduction and valence bands have small but finite overlap; the lack of a full band-gap implies that any topological states that might exist in a semimetal should be distinct from the topological states studied in insulating materials. Theory has proposed two kinds of topological semimetals: the topological Dirac and Weyl semimetals (*2*, *7*–*12*). Their low-energy bulk excitations are described by the Dirac and Weyl equations, respectively. For both types, the bulk conduction and valence bands are predicted to touch at multiple discrete points in the bulk Brillouin zone


[1]Joseph Henry Laboratory, Department of Physics, Princeton University, Princeton, NJ 08544, USA. [2]Princeton Center for Complex Materials, Princeton Institute for Science and Technology of Materials, Princeton University, Princeton, NJ 08544, USA. [3]Department of Chemistry, Princeton University, Princeton, NJ 08544, USA. [4]Center for Condensed Matter Sciences, National Taiwan University, Taipei 10617, Taiwan. [5]Department of Physics, National Tsing Hua University, Hsinchu 30013, Taiwan. [6]Institute of Physics, Academia Sinica, Taipei 11529, Taiwan. [7]Department of Physics, National Sun Yat-Sen University, Kaohsiung 804, Taiwan. [8]Graphene Research Centre and Department of Physics, National University of Singapore 117542. [9]National Synchrotron Radiation Research Center, Taiwan.
*These authors contributed equally to this work. †Corresponding author. E-mail: mzhasan@princeton.edu

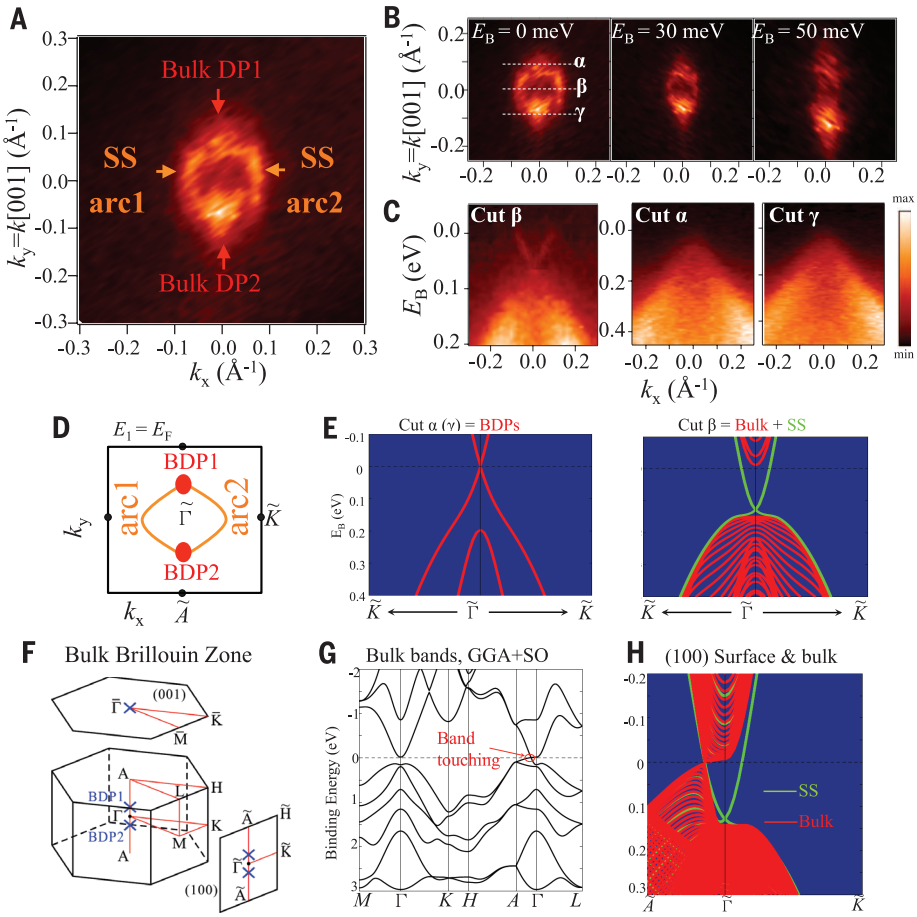


**Fig. 1. Observation of Fermi arc surface states.** (**A**) Fermi surface map of the $Na_3Bi$ sample at photon energy 55 eV. BDP1 and BDP2 denote the two bulk Dirac points. (**B**) ARPES constant energy contours as a function of binding energy at photon energy 55 eV. The dotted lines indicate the momentum space cuts shown in (C). (**C**) ARPES dispersion cuts α, β, and γ as defined in (B) at photon energy 55 eV. (**D**) Schematic Fermi surface of $Na_3Bi$. The red shaded areas and the orange lines represent the bulk and surface states, respectively. (**E**) Calculated band structure along cut β and cut α(γ). (**F**) The bulk BZ and surface BZs of the (001) and (100) surfaces. Bulk Dirac nodes are marked by blue crosses. (**G**) First-principles bulk band calculation for $Na_3Bi$. GGA+SO means that the calculations are based on the generalized gradient approximation (GGA) method in the presence of spin-orbit (SO) coupling. (**H**) First-principles calculation of the (100) surface electronic structure.

(BZ) and show linear behavior in the vicinity of those points (*2*, *7*–*12*). For topological Dirac semimetal material candidates (*9*, *10*), theoretical calculations (*9*–*11*) show that the surface states are a pair of Fermi arcs (Fermi arc surface states) that connect the bulk bands at the energy of the bulk Dirac nodes, which can be realized at the sample's native chemical potential. These double Fermi arc surface states are disjoint on the surface, and they connect to each other through the bulk bands. Moreover, they are predicted to show a wide range of exotic properties, such as unusual polarization (*13*), Friedel oscillations in tunneling experiments (*6*), and novel quantum oscillations in transport (*12*). However, they have not yet been observed in real materials.

Experimentally, a number of compounds have been identified to be three-dimensional (3D) Dirac semimetals (or 3D analogs of graphene), such as $BiTl(S_{0.5}Se_{0.5})_2$, $(Bi_{0.94}In_{0.06})_2Se_3$, $Bi_{1-x}Sb_x$, $Na_3Bi$, and $Cd_3As_2$ (*20*–*25*). Only the latter two are theoretically believed to be topologically nontrivial (*2*), but existing experimental data (*20*–*25*) are insufficient to prove their topological nature. We experimentally uncovered the nontrivial topological nature of the semimetal $Na_3Bi$. We achieved this by observing a pair of spin-polarized Fermi arc surface states at the native Fermi level on the surface of our samples using high-resolution angle-resolved photoemission spectroscopy (ARPES). Our observation of Fermi arc surface states lays the foundation for studying fundamentally new physics in nontrivial metals and may also have potential for device applications (*1*, *2*, *4*–*15*).

$Na_3Bi$ is a semimetal that crystalizes in the hexagonal $P6_3/mmc$ crystal structure with $a$ = 5.448 Å and $c$ = 9.655 Å (*26*). First-principles bulk band calculations (*9*) show that its lowest bulk conduction (Na 3*s*) and valence (Bi $6p_{x,y,z}$) bands possess a band inversion of about 0.3 eV at the bulk BZ center Γ (*9*). The strong spin-orbit coupling in the system can open up energy gaps between the inverted bulk bands, but because of the protection of an additional threefold rotational symmetry along the [001] crystalline direction, the bulk bands are predicted to touch in two locations (Dirac nodes), even after spin-orbit coupling is considered (Fig. 1F, blue crosses). At the (001) surface, because the two bulk Dirac nodes project onto the same point in the surface BZ (Fig. 1F), Fermi arc surface states are not possible at the (001) surface. On the other hand, at the (100) surface, the two bulk Dirac nodes are separated on the opposite sides of the (100) surface BZ center $\bar{\Gamma}$ (Fig. 1F). Consequently, the Fermi arc surface states connecting the bulk Dirac nodes are found in the (100) surface electronic structure calculation (Fig. 1H). In order to experimentally search for the Fermi arc surface states and to probe the topological number for the Dirac semimetal state in $Na_3Bi$, we systematically studied its electronic structure and spin polarization at the (100) side-surface.

Figure 1A shows the ARPES-measured Fermi surface of our $Na_3Bi$ sample at its native Fermi level. The measured Fermi surface consists of two Fermi "points" along the $k_{y[001]}$ direction and two arcs that connect the two Fermi points. We then studied the evolution of constant energy contour as a function of binding energy $E_B$ (Fig. 1B). As we moved $E_B$ below the Fermi level, the two bulk Dirac points were found to enlarge into contours (hole-like behavior), whereas the two surface Fermi arcs shrank (electron-like behavior). In Fig. 1C, we show the energy dispersion for important momentum space cut directions (Fig. 1B). Surface states with a surface Dirac crossing are clearly observed near the Fermi level in cut β. On the other hand, for cuts α and γ, no surface states are observed but the bulk linear band is seen to cross the Fermi level (Fig. 1E). All these ARPES results regarding the band behavior (Fermi surface, electron- or hole-like behavior for each band, and energy dispersion cuts) are in qualitative agreement with the theoretical prediction (*9*). Therefore, our ARPES data demonstrate that the Fermi surface of $Na_3Bi$ is described by two Fermi arc

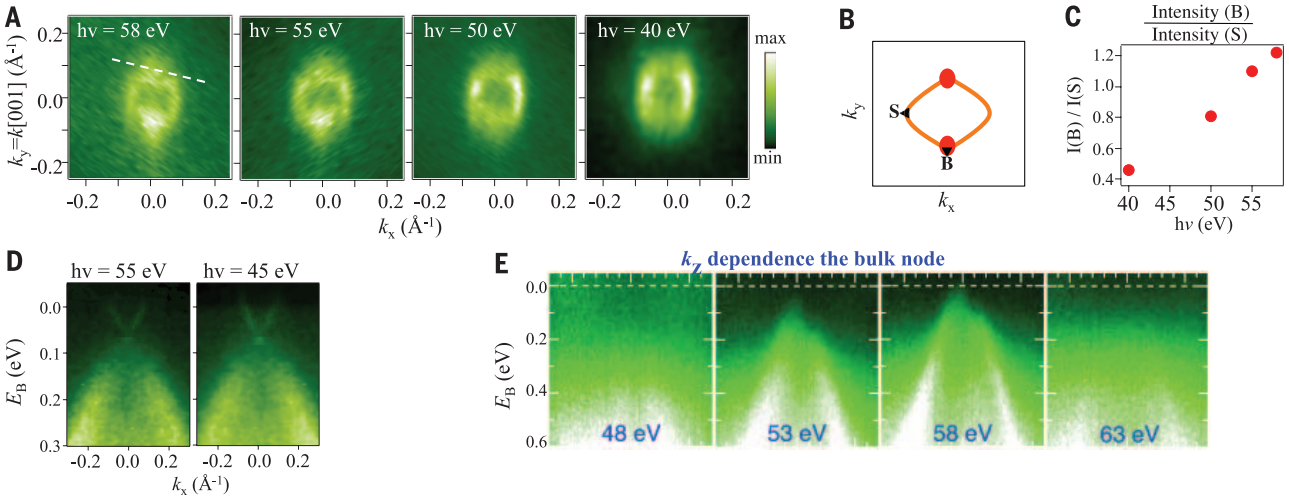


**Fig. 2. Systematic studies of the double Fermi arc surface states.** (**A**) ARPES Fermi surface maps at different photon energies. (**B** and **C**) We denote the middle point of the left Fermi arc as "S" and the bottom bulk Dirac point as "B." (C) shows the relative ARPES intensity between "S" and "B." (**D**) ARPES dispersion maps of the surface states at two different photon energies. (**E**) ARPES dispersion maps of the bulk Dirac band at different photon energies, along the cut indicated by the white dotted lines in (A).

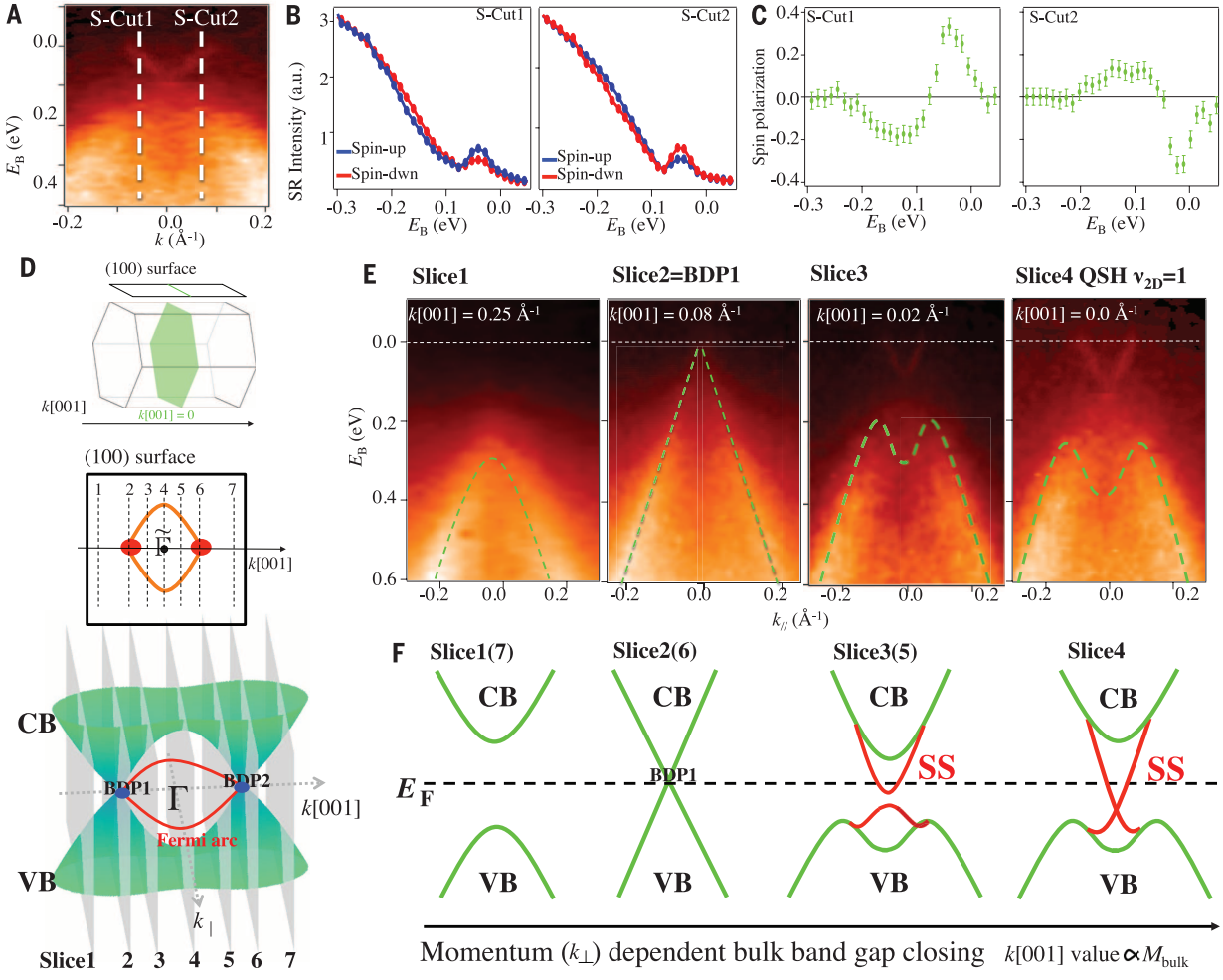


**Fig. 3. Surface spin polarization and the 2D topological number.** (**A**) The white dotted lines indicate the two momenta chosen for spin-resolved measurements. (**B** and **C**) Spin-resolved ARPES intensity and net spin polarization along the in-plane tangential direction for S-cuts 1 and 2 at photon energy 55 eV. The error bars in (C) show the experimental uncertainty in determining the magnitude of the spin polarization. (**D**) A schematic view of the band structure of the topological Dirac semimetal phase. Seven 2D-*k* slices that are taken perpendicular to the $k_{[001]}$ axis are noted. (**E** and **F**) ARPES-measured [(E)] and schematic [(F)] band structure for these slices are shown.

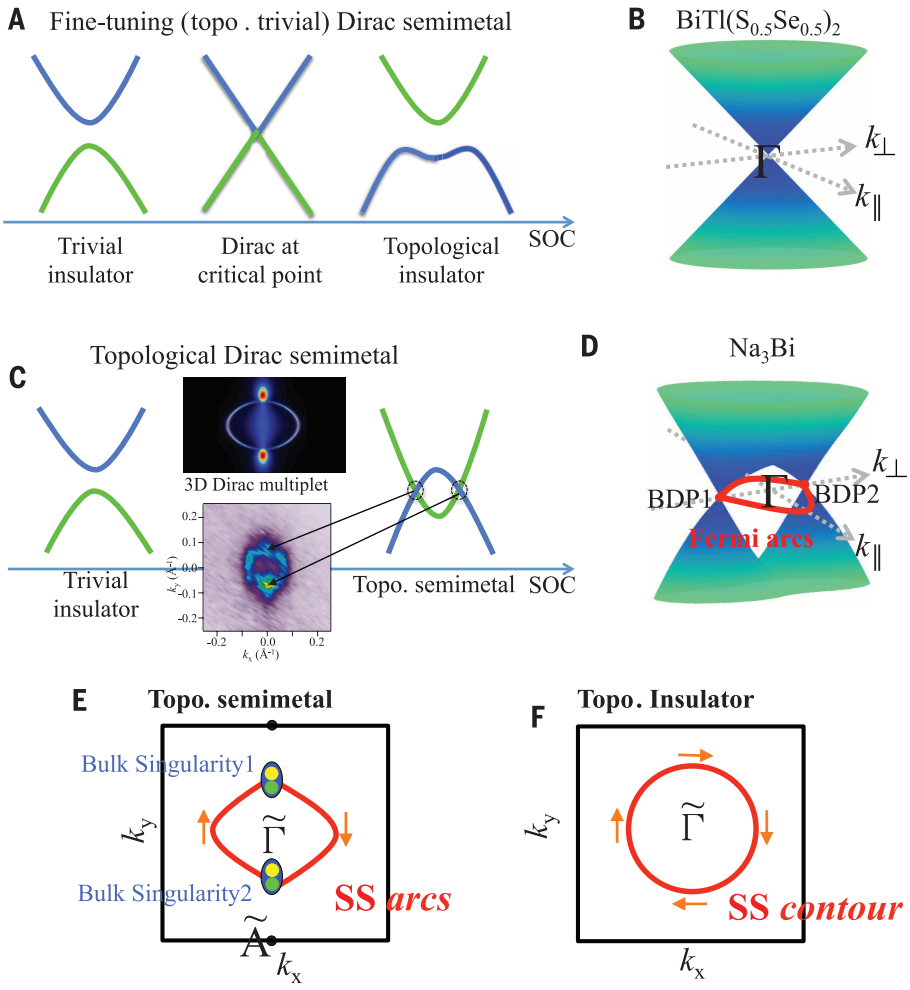


**Fig. 4. Comparison between a trivial 3D Dirac semimetal achieved by fine tuning and a topological Dirac semimetal.** (**A**) A 3D Dirac semimetal state with only one bulk Dirac cone can be realized by tuning a system to the critical point of a topological phase transition between a band insulator and a topological insulator. (**B**) Schematic band structure of $BiTl(S_{0.5}Se_{0.5})_2$, which is at the critical composition of the topological phase transition system (*20*). (**C**) A topological Dirac semimetal phase is realized in an inverted band structure and is stable without fine tuning because of additional protection by crystalline symmetries. (**D**) Schematic band structure from the (100) surface of a topological Dirac semimetal. In this schematic, only surface states at the bulk Dirac point energy are plotted. Surface states at other energies are not shown. (**E** and **F**) Schematic Fermi surface of $Na_3Bi$ and $Bi_2Se_3$. In $Na_3Bi$, each Dirac node (the blue shaded area) can be viewed as a composite of two degenerate Weyl nodes (yellow and green areas). The orange arrows note the spin polarization according to our spin-resolved ARPES measurements. The inset of (C) shows the ARPES-measured Fermi surface.

surface states that connect two bulk Dirac nodes at our samples' native chemical potential.

In order to further confirm the 2D surface nature for the double Fermi arc surface states and the 3D bulk nature for the two bulk Dirac bands, we present Fermi surface maps at different incident photon energies. The double Fermi arcs are observed at all photon energies, whereas the bulk Dirac nodes are pronounced only at 55 to 58 eV (Fig. 2, A to C). Furthermore, we show the dispersion along cut β, which also confirms that the surface state spectra do not depend on photon energy (Fig. 2D). In contrast, the bulk Dirac bands disperse strongly in photon energy (Fig. 2E). The systematic photon energy ($k_z$)–dependent data in Fig. 2 clearly demonstrate that the electronic states at the Fermi level are localized at the surface (2D surface state nature) everywhere around the Fermi surface contour, except at the locations of the two bulk Dirac nodes, where the states disperse strongly in all three dimensions (3D bulk band nature).

Next, we studied the surface spin polarization along cut β, where a surface Dirac crossing within the bulk bandgap is observed. Figure 3, B and C, show the in-plane spin-resolved intensity and net spin polarization. The direction of spin polarization is reversed upon going from S-cut 1 to S-cut 2 (defined in Fig. 3A), which shows the spin-momentum locking property and the singly degenerate nature of the Fermi arc surface states along the cut β direction.

We used the observed electronic and spin structure for the (100) Fermi arc surface states to obtain the topological number for the Dirac semimetal state in $Na_3Bi$. Because of the existence of the two bulk nodes (slices 2 and 6), our ARPES data (Fig. 3, D and E) show that the bulk bandgap closes and reopens as one goes across each bulk node (slice 2 or 6). We carefully examined the ARPES electronic structure for all 2D-$k$ slices, where the bulk is gapped (slices 1, 3 to 5, and 7). It can be seen from Fig. 3, E and F, that slices 1 and 7 are gapped without any surface states; slices 3 and 5 do have surface states, but the surface states are gapped and do not connect across the bulk bandgap; however, for slice 4 ($k_{[001]} = 0$), our data show gapless Dirac surface states that span across the bulk gap. Therefore, our data indicate that slice 4 has a nontrivial 2D topological number. Because slice 4 (the $k_{[001]} = 0$ plane) is invariant under the time-reversal operation, it is possible for slice 4 to have a nonzero 2D $\mathbb{Z}_2$ number $\nu_{2D} = 1$ (*2*, *14*, *15*). If that is the case, then slice 4 can be viewed as a 2D quantum spin Hall-like system, and one would expect a Dirac surface state with a helical spin texture connecting the bulk conduction and valence bands. Indeed, this is what we observe in our ARPES (Fig. 3E) and spin-ARPES (Fig. 3, A to C) data. Therefore, our data demonstrate that $Na_3Bi$ is a topological Dirac semimetal that features a 2D topological number $\nu_{2D} = 1$ for the $k_{[001]} = 0$ plane, which is consistent with the prediction in (*2*). Further elaborations regarding the topological properties of $Na_3Bi$ are presented in the supplementary materials (figs. S1 and S2). Figure 4, A to D, shows schematically the difference between a trivial and topological Dirac semimetal.

Our observations of topological surface states, the way in which they connect to the bulk Dirac cones, and their spin momentum locking demonstrate the topology of a Dirac semimetal in line with the theoretical prediction (*2*). The observed Fermi arc surface states represent a type of 2D electron gas that is distinct from that of the surface states in a $\mathbb{Z}_2$ topological insulator (*27*). In a typical topological insulator such as $Bi_2Se_3$, the surface states' Fermi surface is a closed contour. In sharp contrast, the Fermi surface in $Na_3Bi$ consists of two arcs, which are bridged by the two bulk nodes (Fig. 4, E and F). Therefore, as one goes along the surface Fermi arc and reaches a bulk node, the wave function of the

surface state gradually loses its surface nature and becomes a bulk band. Such exotic behavior does not exist in surface states of $Bi_2Se_3$ or any known topological insulator. In surface electrical transport experiments at high magnetic field, it would be interesting to study how the surface electrons wind along the arc and enter the bulk singularity as considered by a recent theoretical work (*5*), if the chemical potential can be placed precisely at the bulk Dirac node so that the bulk carrier density is vanishingly small (*5*). Finally, it would be interesting to introduce superconductivity or magnetism in these new topological metals (*9*, *10*, *28*). In particular, breaking time-reversal symmetry via magnetism can split the Dirac nodes into Weyl nodes (Fig. 4E).

## REFERENCES AND NOTES


1. A. M. Turner, A. Vishwanath, http://arxiv.org/abs/1301.0330 (2013).
2. B.-J. Yang, N. Nagaosa, *Nat. Commun.* **5**, 4898 (2014).
3. M. Z. Hasan, S.-Y. Xu, M. Neupane, http://arxiv.org/abs/1406.1040 (2014).
4. F. D. M. Haldane, http://arxiv.org/abs/1401.0529 (2014).
5. A. C. Potter, I. Kimchi, A. Vishwanath, *Nat. Commun.* **5**, 5161 (2014).
6. P. Hosur, *Phys. Rev. B* **86**, 195102 (2012).
7. S. Murakami, *New J. Phys.* **9**, 356 (2007).
8. S. M. Young *et al*., *Phys. Rev. Lett.* **108**, 140405 (2012).
9. Z. Wang *et al*., *Phys. Rev. B* **85**, 195320 (2012).
10. Z. Wang, H. Weng, Q. Wu, X. Dai, Z. Fang, *Phys. Rev. B* **88**, 125427 (2013).
11. A. Narayan, D. Di Sante, S. Picozzi, S. Sanvito, http://arxiv.org/abs/1408.3509 (2014).
12. X. Wan, A. M. Turner, A. Vishwanath, S. Y. Savrasov, *Phys. Rev. B* **83**, 205101 (2011).
13. T. Ojanen, *Phys. Rev. B* **87**, 245112 (2013).
14. M. Z. Hasan, C. L. Kane, *Rev. Mod. Phys.* **82**, 3045–3067 (2010).
15. J. E. Moore, *Nat. Phys.* **5**, 378–380 (2009).
16. D. Hsieh *et al*., *Nature* **452**, 970–974 (2008).
17. D. Hsieh *et al*., *Science* **323**, 919–922 (2009).
18. Y. Xia *et al*., *Nat. Phys.* **5**, 398–402 (2009).
19. X.-G. Wen, *Phys. Rev. B* **89**, 035147 (2014).
20. S.-Y. Xu *et al*., *Science* **332**, 560–564 (2011).
21. M. Brahlek *et al*., *Phys. Rev. Lett.* **109**, 186403 (2012).
22. S.-Y. Xu *et al.*, http://arxiv.org/abs/1312.7624 (2013).
23. Z. K. Liu *et al*., *Science* **343**, 864–867 (2014).
24. M. Neupane *et al*., *Nat. Commun.* **5**, 3786 (2014).
25. S. Borisenko *et al*., *Phys. Rev. Lett.* **113**, 027603 (2014).
26. T. B. Massalski, *Binary Alloy Phase Diagrams* (ASM, Materials Park, OH, ed. 2, 1990).
27. M. Z. Hasan, www.fysik.su.se/~ardonne/nobel/ns156-program.pdf (2014).
28. S. A. Yang, H. Pan, F. Zhang, *Phys. Rev. Lett.* **113**, 046401 (2014).


## ACKNOWLEDGMENTS


The work at Princeton and Princeton-led synchrotron-based ARPES measurements are supported by U.S. Department of Energy grant DE-FG-02-05ER46200. H.L. acknowledges the Singapore National Research Foundation (NRF) for support under NRF award no. NRF-NRFF2013-03. C.-Y.H. and W.-F.T. are supported by the Ministry of Science and Technology (MOST) in Taiwan under grant no.103-2112-M-110-008-MY3. T.-R.C. and H.-T.J. are supported by the National Science Council, Taiwan. H.-T.J. also thanks the National Center for High-Performance Computing, Taiwan; the Computer and Information Network Center–National Taiwan University, Taiwan; and the National Center for Theoretical Sciences, Taiwan, for technical support. Crystal growth was supported by the Army Research Office Multidisciplinary University Research Initiative on topological insulators, grant no. W911NF-12-1-0461. F.-C.C acknowledges the support provided by MOST-Taiwan under project number 103-2119-M-002-020-MY3. G.B. is supported by grant NSF-DMR-1006492. We gratefully acknowledge M. Leandersson, C. M. Polley, J. Adell, T. Balasubramanian, K. Miyamoto, T. Okuda, and M. Hashimoto for their beamline assistance at the Maxlab, the Hiroshima Synchrotron Radiation Center (Hisor), and the Stanford Synchrotron Radiation Lightsource (SSRL). We also thank C. Fang, B. A. Bernevig, and A. Vishwanath for discussions. ARPES data were collected at the beamline 5-4 at the SSRL at the Stanford Linear Accelerator Center in California, USA; the beamlines I3 and I4 at the MAX-lab in Lund, Sweden; and the beamline-9B of the Hisor in Hiroshima, Japan.


## SUPPLEMENTARY MATERIALS

www.sciencemag.org/content/347/6219/294/suppl/DC1
Materials and Methods
Figs. S1 and S2
References (*29*–*31*)


30 May 2014; accepted 9 December 2014
Published online 18 December 2014;
10.1126/science.1256742

# Observation of Fermi arc surface states in a topological metal

Su-Yang Xu *et al.*

*Science* **347**, 294 (2015);
DOI: 10.1126/science.1256742